BRAIN CONNECTIVITY
Volume 3, Number 6, 2013

DOI: 10.1089/brain.2013.0175

Resting-State Networks and the Functional Connectome of the Human Brain in Agenesis of the Corpus Callosum

Julia P. Owen,[1,*] Yi-Ou Li,[1,*] Fanpei G. Yang,[1,2] Charvi Shetty,[1] Polina Bukshpun,[3] Shivani Vora,[3] Mari Wakahiro,[3] Leighton B.N. Hinkley,[1] Srikantan S. Nagarajan,[1,4] Elliott H. Sherr,[3] and Pratik Mukherjee[1,4]

Abstract

The corpus callosum is the largest white matter fiber bundle connecting the two cerebral hemispheres. In this work, we investigate the effect of callosal dysgenesis on functional magnetic resonance imaging (fMRI) resting-state networks and the functional connectome. Since alternate commissural routes between the cerebral hemispheres exist, we hypothesize that bilateral cortical networks can still be maintained in partial or even complete agenesis of the corpus callosum (AgCC). However, since these commissural routes are frequently indirect, requiring polysynaptic pathways, we hypothesize that quantitative measurements of interhemispheric functional connectivity in bilateral networks will be reduced in AgCC compared with matched controls, especially in the most highly interconnected cortical regions that are the hubs of the connectome. Seventeen resting-state networks were extracted from fMRI of 11 subjects with partial or complete AgCC and 11 matched controls. The results show that the qualitative organization of resting-state networks is very similar between controls and AgCC. However, interhemispheric functional connectivity of precuneus, posterior cingulate cortex, and insular-opercular regions was significantly reduced in AgCC. The preserved network organization was confirmed with a connectomic analysis of the resting-state fMRI data, showing five functional modules that are largely consistent across the control and AgCC groups. Hence, the reduction or even complete absence of callosal connectivity does not affect the qualitative organization of bilateral resting-state networks or the modular organization of the functional connectome, although quantitatively reduced functional connectivity can be demonstrated by measurements within bilateral cortical hubs, supporting the hypothesis that indirect polysynaptic pathways are utilized to preserve interhemispheric temporal synchrony.

Key words: brain development; connectivity; connectome; corpus callosum; fMRI; graph theory; malformations; white matter

Introduction

Functionally connected networks of cortical regions in the human brain can be defined by the temporal synchrony of the blood oxygenation level-dependent (BOLD) signals observed in resting-state functional magnetic resonance imaging (fMRI) (Damoiseaux *et al.* 2006; Greicius *et al.*, 2003). Resting-state networks can be derived from spontaneous BOLD fluctuations using data-driven methods such as independent component analysis (ICA) (Beckmann and Smith, 2004; Damoiseaux *et al.*, 2006; McKeown *et al.*, 1998), as well as hypothesis-driven techniques such as seed-based correlation (Biswal *et al.*, 1995; Greicius *et al.*, 2003). These intrinsically connected cortical networks at rest have been shown to be similar to the networks activated by task-related fMRI paradigms (Smith *et al.*, 2009). Functional connectomics is a complementary analytic approach that applies graph theory to a "whole-brain network" which encompasses the resting-state BOLD coupling among all cortical regions. Noninvasive mapping of the structural connectome in the human brain has been enabled by diffusion-weighted MRI and tractography (Basser *et al.*, 2000). Graph theoretic analysis of whole-brain tractography has shown that axonal pathways form "small-world networks" (Hagmann *et al.*, 2008) and that many of the highly connected regions or "hubs" of the structural network overlap cortical regions which are highly active in the

[1]Department of Radiology and Biomedical Imaging, University of California, San Francisco, California.
[2]Department of Foreign Languages and Literatures, National Tsinghua University, Hsinchu, Taiwan.
[3]Department of Neurology and [4]Graduate Program in Bioengineering, University of California, San Francisco, California.
*These authors contributed equally to this work.

resting-state, that is, the default mode network (Greicius *et al.*, 2003; Hagmann *et al.*, 2008; Raichle *et al.*, 2001; van den Heuvel and Sporns, 2011). The relationship between structural connectivity and functional connectivity in the human brain is an area of active investigation, as it is clear from direct comparisons that, while they are strongly correlated, there is no one-to-one correspondence (Damoiseaux and Greicius, 2009; Greicius *et al.*, 2009; Honey *et al.*, 2009, 2010, Skudlarski *et al.*, 2008).

In this work, we examine how structural connectivity across the corpus callosum affects the resting-state BOLD connectivity of cortical networks and the functional connectome. The great majority of fMRI resting-state networks, as assessed by ICA or seed-based correlation, are bihemispheric and most show a high degree of bilateral symmetry (Damoiseaux *et al.*, 2006). Cortical modules from functional connectomic analysis are also strikingly bilaterally symmetric (He *et al.*, 2009). Therefore, these intrinsically connected networks presumably require interhemispheric communication in order to maintain temporal synchrony of the BOLD signal. The corpus callosum is, by far, the largest commissural white matter tract in the human brain and contains almost all of the interhemispheric fiber pathways between neocortical regions (Aboitiz *et al.*, 1992). A natural way to investigate the influence of callosal structural connectivity on interhemispheric functional connectivity is through the study of individuals who are born without a corpus callosum (Paul *et al.*, 2007), a condition known as agenesis of the corpus callosum (AgCC). It has recently been demonstrated that bilateral resting-state networks from BOLD fMRI are qualitatively intact in high-functioning individuals with AgCC (Li *et al.*, 2011; Tyszka *et al.*, 2011), despite the complete absence of callosal connectivity. This surprising result likely reflects the effect of indirect routes between the cerebral hemispheres, such as through the anterior commissure, hippocampal commissure, and posterior commissure. However, information transmission via these polysynaptic interhemispheric pathways is not as rapid as that through monosynaptic callosal routes. Therefore, we hypothesize that quantitative comparisons of functional connectivity in these networks will reveal decreased interhemispheric connectivity in AgCC. These reductions would be expected to be greatest at the most highly interconnected cortical regions of the two cerebral hemispheres, such as the hubs of the default mode network (Hagmann *et al.*, 2008). These data may help elucidate the relationship between structural and functional connectivity in the normal human brain as well as aid in explaining the characteristic neurobehavioral features typical of acallosal individuals (Paul *et al.*, 2007).

Materials and Methods

Subjects

Eleven individuals with AgCC (seven complete and four partial) and 11 normal controls were prospectively enrolled. The T1-weighted MR images of the four partial AgCC and one representative complete AgCC subjects are presented with midline sagittal view in Figure 1. The two groups did not differ significantly ($p > 0.05$) with regard to mean age (AgCC: 27.3 ± 9.6 years; controls: 30.2 ± 10.3 years), gender distribution (AgCC: 10 male; controls: 9 male), or mean Wechsler Adult Intelligence Scale full-scale IQ (AgCC: 93.5 ± 12.8; controls: 101.1 ± 18.2). All of the control subjects were right-handed, while the AgCC group was composed of six right-handed and five left-handed individuals.

Image acquisition

All subjects were studied at three Tesla (GE Healthcare, Waukesha, WI) using an 8-channel head coil. A 7 min BOLD fMRI multislice gradient echo echoplanar acquisition used an FOV 22×22 cm, 64×64 matrix, 4 mm interleaved slices with no gaps, and repetition time (TR) of 2 sec and echo time (TE) of 28 msec. After 10 dummy volumes to reach equilibrium longitudinal magnetization, 200 volumes were collected with the subject's eyes closed to minimize exogenous visual activation and with instructions to remain awake. Structural imaging was performed using an axial 3D inversion recovery fast spoiled gradient echo T1-weighted sequence (TE = 1.5 msec, TR = 6.3 msec, inversion time 400 msec, flip angle of 15 degrees) with 230 mm FOV, 156 1.0-mm contiguous partitions at a 256×256 matrix.

Preprocessing

Motion correction was applied to fMRI volume data by registering each scanned volume data with the median

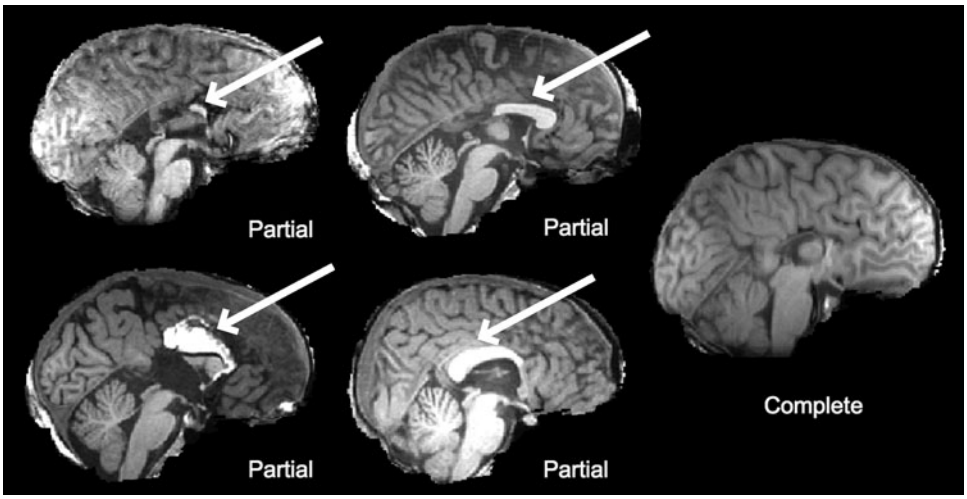

FIG. 1. Midline sagittal view of the T1-weighted images of four partial agenesis of the corpus callosum (AgCC) patients and one complete AgCC patient. Arrows point to the callosal fragment present in each partial AgCC subject.

volume using the "mcflirt" function with six degrees of freedom supplied in the FMRIB Software Library (FSL) (www.fmrib.ox.ac.uk/fsl) toolbox. In-brain voxels were extracted using the "bet" function in FSL. The fMRI image of each subject was first registered to the same subject's T1-weighted image; then, the T1-weighted image was registered to the MNI152 2 mm standard template using the "flirt" function in FSL toolbox with default settings. The transformation in the latter step was applied to the registered fMRI image in the first step to obtain the fMRI images registered to the MNI152 atlas space using the "flirt" function. Spatial smoothing was applied by spatially convolving each fMRI volume with a $5\times5\times5$ mm Gaussian kernel, using the "fslmaths" function in FSL. In this study, we registered the T1 and fMRI images of both AgCC and control subjects onto the MNI T1-weighted template. For quality check, we overlaid registered T1-weighted images onto the MNI template to make sure that the gray matter areas are properly aligned for the registered T1 images as shown in Figure 2 for a representative AgCC case. BOLD fMRI images have poor gray-white matter contrast compared with the T1-weighted images that form the basis of the MNI152 template; hence, it is not feasible to directly compare co-registered fMRI images against the MNI template on structural details. Therefore, we take the temporal standard deviation across all 200 fMRI volumes at each voxel to compute the standard deviation map of the fMRI data. This map shows better gray-white contrast and is in the same space as the fMRI image. We show the standard deviation map of the co-registered fMRI and compare it with the target MNI152 image in Figure 3 for a representative AgCC case.

For seed-region correlation analysis, motion correction was applied to fMRI volumes by registering each scanned volume with the median volume using the "mcflirt" function with six degrees of freedom supplied in the FSL toolbox. The standard deviation image volume from all 200 time points of the resting-state fMRI for each subject was first registered to the same subject's T1-weighted image volume with the transformation saved for registration to the MNI template in a later step. Temporal band-pass filtering was applied to each voxel time series with the pass band from 0.010 to 0.125 Hz. Linear regression was applied to the fMRI time series at each voxel to regress out a constant baseline, a linear trend, the six motion parameters from motion correction, and the mean time series from white matter and cerebral spinal fluid mapped from T1-weighted image segmentation. The transformations obtained for fMRI to T1 and T1 to MNI template registration were concatenated to transform the fMRI images to the MNI atlas space. Spatial smoothing was applied by convolving each fMRI volume with a $5\times5\times5$ mm Gaussian kernel.

Data analysis

Independent component analysis. The Group ICA of fMRI toolbox (GIFT) was used with the recommended settings of intensity normalization option and ICA3 group dimension reduction (Calhoun *et al.*, 2001; Erhardt *et al.*,

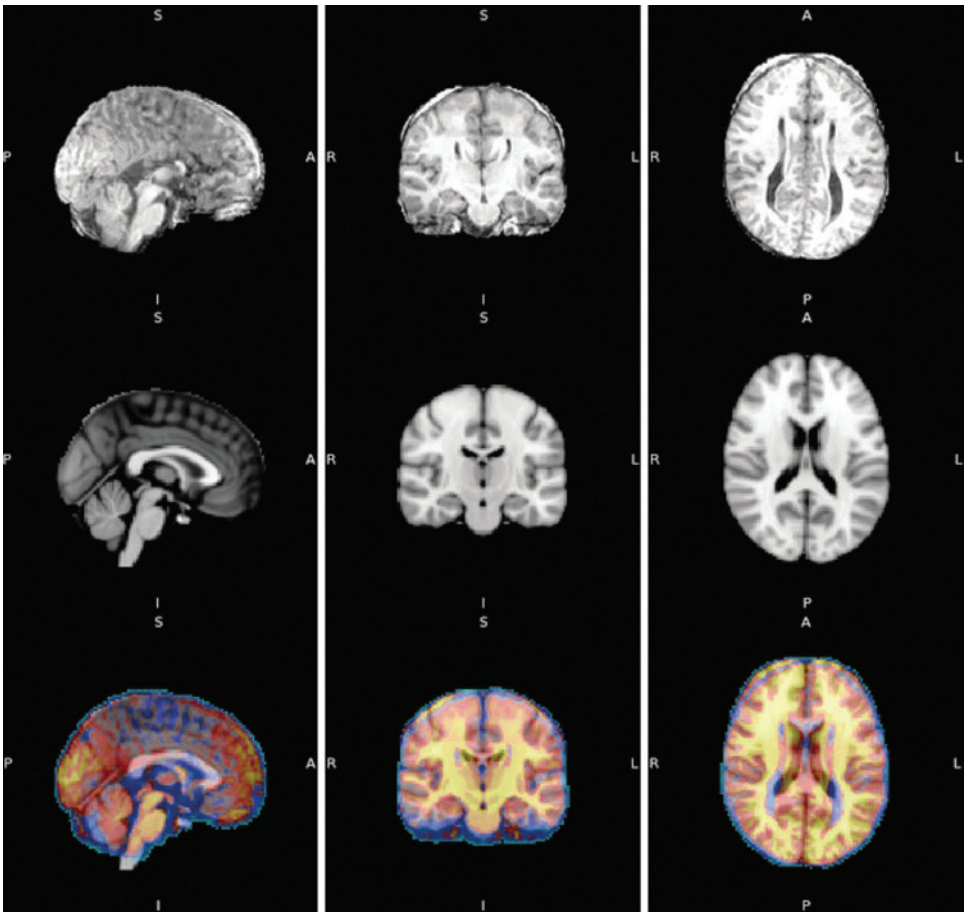

FIG. 2. Registered T1 image of an AgCC subject (top), the MNI152_T1_2 mm template (center) and registered T1 image of AgCC subject overlaid onto MNI152_T1_2 mm with the blue-red-yellow contrast represents the registered AgCC subject T1 image, the underlying gray contrast is the MNI15_T1 template (bottom).

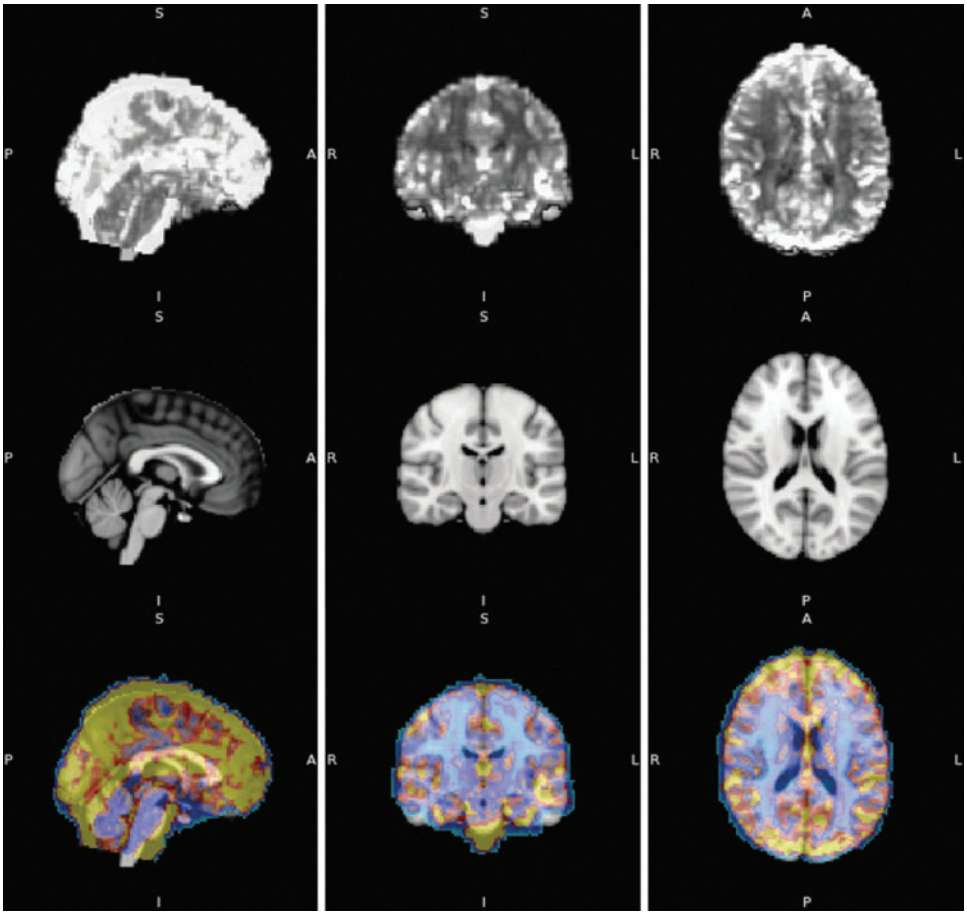

FIG. 3. Standard deviation map of the registered fMRI image of an AgCC subject (top), the MNI152_T1_2 mm template (center) and standard deviation map of AgCC subject overlaid onto MNI152_T1_2 mm with the blue-red-yellow contrast represents the registered AgCC subject T1 image, the underlying gray contrast is the MNI15_T1 template (bottom).

2010). The Infomax algorithm (Bell and Sejnowski, 1995) was used to estimate 25 independent component (IC) spatial maps. We ran the GIFT order selection to estimate the number of components of each subject subjects' dataset. The estimated number of components for the 22 subjects ranged from 32 to 63. Since GIFT performs an ICA decomposition on the aggregated data, it is reasonable to be conservative and stay with the lowest order (i.e., the number of components that every subject can support). We further reduced the number of ICs to increase the stability of the IC estimates.

After ICA decomposition of group-aggregated data, ICs for each individual subject were back-reconstructed in GIFT in order to perform group-level comparisons on each component. A voxel-wise one-sample nonparametric permutation test was performed on the back-reconstructed IC maps of the 22 subjects for each IC using the "randomize" function in FSL with 5000 permutations (Smith and Nichols, 2009). The significance level of each IC spatial map was thresholded to control the family-wise error rate to be $p < 0.05$. ICs of interest were selected for a further study based on the correspondence of their localized spatial connectivity patterns to previously reported resting-state networks (Damoiseaux *et al.*, 2006).

A voxel-wise nonparametric two-sample inference test with the randomize function was performed to find the statistically significant differences in connectivity maps between the AgCC group and the control group. The maps were thresholded using $p < 0.05$, controlling for the family-wise error rate. The supra-threshold regions on the maps were displayed in color on the anatomical MNI152 template.

Seed-region correlation

To verify the group differences of functional connectivity in those regions identified by group ICA with the voxel-wise two-sample randomized test, we retrieved the original fMRI time series from the regions of interest (ROIs) shown in Figure 2 and performed a confirmatory seed region correlation analysis. To test intra-ROI functional connectivity, we calculated the averaged correlation coefficients between fMRI time series from all pairs of voxels in the bilateral ROI as well as separately from ROIs confined to the left or right hemisphere. For IFC, the actual time series were extracted from the ROIs in the left and right hemisphere, and the IFC correlation coefficient was then calculated between the averaged time series from the ROIs in each hemisphere. A two-tailed two-sample *t*-test was applied to the Fisher-transformed intra-ROI correlations and IFC correlation values to determine statistically significant differences between the AgCC and control groups.

Connectomics

To evaluate the overall network topology of BOLD functional connectivity in AgCC, we adopt a graph theoretic approach. The mean time course was extracted from 90 cortical and subcortical ROIs from the automatic anatomic labeling

(AAL) atlas (excluding the cerebellar regions). The Pearson correlation coefficient was computed between each pair of ROIs. Compiling all the correlation coefficients results in an *adjacency matrix* that denotes the strength of the temporal coupling (edges) between each pair of regions (nodes). The adjacency matrix for each subject was then thresholded to obtain binary matrices of a desired density of the network, varying from 10% to 40% of all possible pairwise connections. We do not include negative correlations in the individual adjacency matrices, as these are not easily interpreted and could be spurious (Saad *et al.*, 2012; Yan *et al.*, 2013). Eight commonly used graph metrics were computed to summarize properties of the binary networks as a function of density. We computed three variants of degree: (1) degree accounting for only interhemispheric connections, (2) degree accounting for only left intrahemispheric connections, and (3) degree accounting for only right intrahemispheric connections. The five additional metrics were characteristic path length, mean normalized betweenness, global efficiency, mean local efficiency, and mean clustering coefficient.

The modular organization of the control and AgCC functional connectomes was computed using a modularity detection algorithm applied to the group-binarized adjacency matrix (Blondel *et al.*, 2008). The group-binarized adjacency matrices were computed for both the control and AgCC groups as in He and associates (2009). In brief, a two-tailed one-sample *t*-test was performed on the Fisher-transformed correlation coefficients. (All correlations, negative and positive, were included in the statistical test across subjects.) Then, a significance level of $p < 0.001$ was employed to threshold the matrix p-values, resulting in a binarized matrix reflecting the group topology. The resulting density of connection of the binary matrices for both the controls and AgCC is $\sim$10%. In a subgroup analysis, a group-binarized adjacency matrix was also calculated for the seven complete AgCC subjects only; in this case, a threshold of $p < 0.01$ was used, resulting in a binary matrix of roughly the same sparsity as the control and AgCC groups. The partition obtained by the module detection algorithm is sensitive to initialization; as such, we ran the algorithm 100 times and chose the partition that was found for the majority of initializations as done in Owen and associates (2013a, 2013b).

Given the modular structure of the controls and AgCC, we next tested whether the connection strengths within the modules differed between groups as done in Meskaldji and colleagues (2011) and Owen and colleagues (2013a). A two-sample Student *t*-test was used on all the Fisher-transformed connection strengths in a particular module and the resulting *p*-values were FDR-corrected, yielding regions in AgCC with increased or decreased coupling as compared with the controls. This procedure was done for the modules defined by both the control and AgCC group-binarized matrices.

Lastly, the edge-space similarity for the controls and AgCC cohorts was computed for the weighted and binarized matrices as in Bassett and colleagues (2011), Wang and colleagues (2011), and Owen and colleagues (2013a, 2013b). For a weighted connectome, a correlation coefficient is computed for the edge weights of two individuals. For the binarized matrices, we first threshold to a density of 0.2 (i.e., 20% of all possible connections) and then compute the fraction of binary edges that agree between two individuals (both 0 or both 1) and normalize by the total number of edges. To assess the relative consistency of different types of connections, we computed the edge-space similarity for (1) all connections, (2) all interhemispheric connections, (3) all intrahemispheric connections, (4) all right intrahemispheric connections, and (5) all left intrahemispheric connections. We assess four groupings of the data: (1) all controls versus AgCC (11 vs. 11), (2) all controls versus complete AgCC (11 vs. 7), (3) all controls versus right-handed AgCC (11 vs. 6), and (4) all controls versus left-handed AgCC (11 vs. 5). The weighted and binary edge-space similarity was computed in a pair-wise fashion between all subjects in each grouping of connections and subjects. The Fisher-transformed values were then used in a two-sample Student *t*-test to assess for group differences.

Voxel-based morphometry

To exclude the possible confounding effect of AgCC structural abnormalities on functional imaging contrast, we performed a VBM analysis of the 3D T1-weighted images of the 11 AgCC subjects and 11 controls. All the T1-weighted images were normalized and smoothed with an 8 mm Gaussian kernel. A voxel-wise two-tailed two-sample *t*-test was performed using SPM5 between AgCC and control groups, restricting the analysis to voxels within a normalized mask derived from the SPM MNI152 T1-weighted template. The FDR correction was set to $p < 0.05$, and contrasts of control > AgCC and AgCC < control were generated.

Confirmatory analysis, ICA, and connectomics. In order to reconcile the ICA and functional connectome results, we performed a final *post hoc* analysis of selected edges in the connectome. We chose regions implicated as having group differences in the ICA analysis, determined the AAL labels that most overlapped these regions, and extracted the edges from the connectome that connect these AAL regions. Then, after Fisher transformation, a two-sample Student *t*-test was used to detect significant differences in the coupling between regions in AgCC as compared to the controls.

Results

ICA of resting-state fMRI

Figure 4 illustrates the 17 IC maps that were identified based on the similarity between their localized spatial connectivity patterns and commonly reported resting-state networks in cortical regions (Damoiseaux, 2006) as well as three IC maps with connectivity patterns in the cerebellum and brainstem. Due to the effect of model order on ICA decomposition (Abou-Elseoud *et al.*, 2010), large-scale networks such as the default mode network split into parts as different ICs in our study. Hence, we include all split components in the subsequent comparisons. Three of the IC spatial maps show significant group differences, specifically bilaterally symmetric decreases of functional connectivity in AgCC subjects compared with controls (Fig. 5). These are the bilateral insular-opercular network (IC21), the inferior part of the posterior cingulate cortex (PCC) bilaterally (IC14), and the bilateral precuneus-PCC (IC18). Another two ICs with predominantly unilateral spatial maps show decreased functional connectivity in AgCC (Fig. 5), although to a lesser degree than the aforementioned three bilateral networks. As shown in Figure 4, these are a right frontoparietal network (IC15), and a left frontoparietal network (IC8).

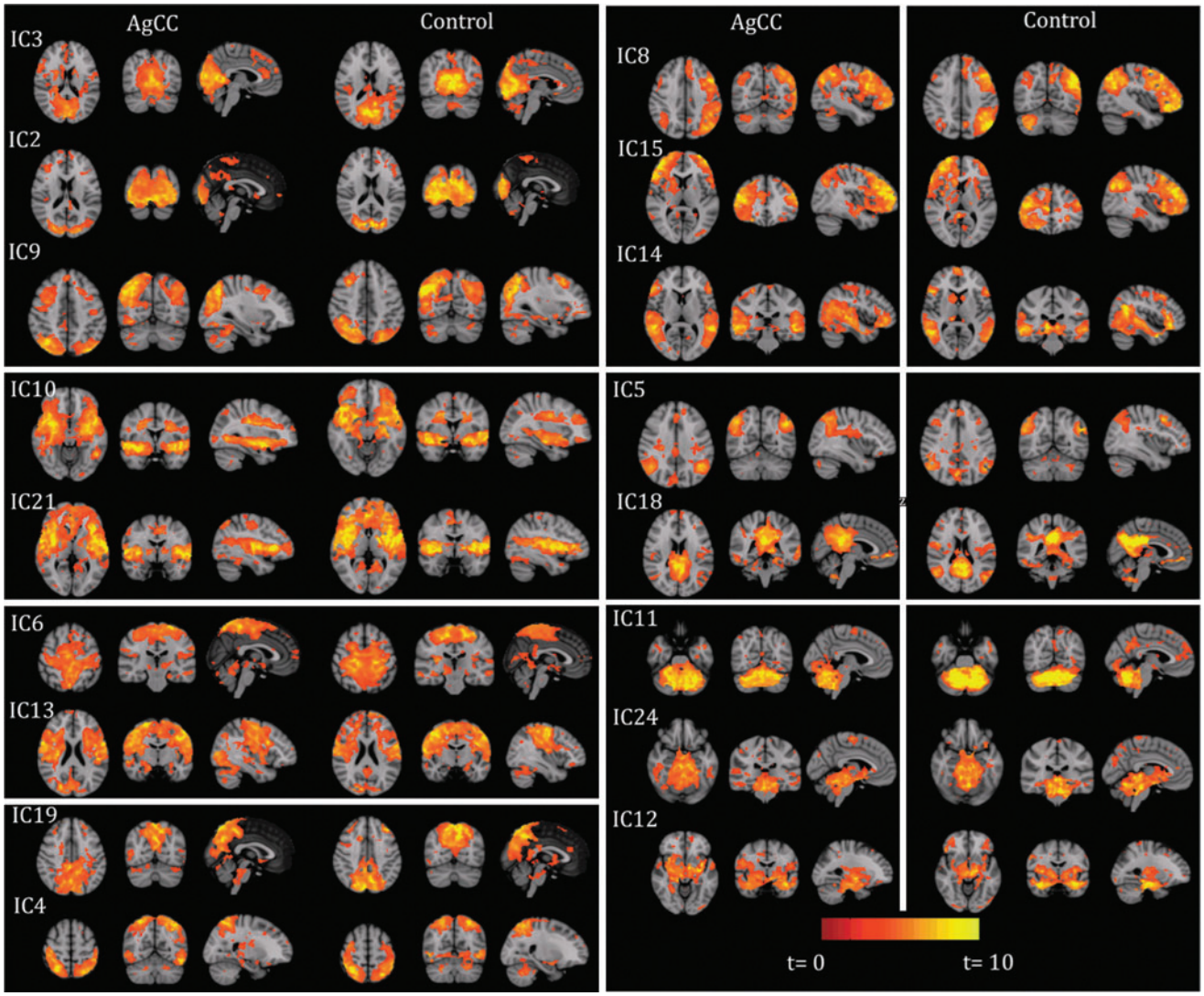

FIG. 4. Comparison between AgCC and normal controls of the resting-state networks estimated by group ICA of BOLD fMRI. Three components showing connectivity in the occipital lobes are the lingual gyri (IC3), the occipital lobules (IC2), and the superior occipital lobules (IC9). Two temporal networks include the inferior temporal lobes (IC3) and superior temporal lobes (IC21). Two sensorimotor maps are seen at the upper motor cortex (IC6), and the pre- and post-central gyri (IC13). Parietal connectivity is observed at the precuneus (IC19) and superior parietal lobes (IC4). Frontal networks include the left frontoparietal regions (IC8), right frontoparietal regions (IC15), and bilateral frontotemporal regions (IC14). Two components show connectivity at the superior part of the default mode network (IC5) and the inferior part of the default mode network (IC18). Three connectivity maps of the posterior fossa are at the cerebellum (IC11), vermis (IC24), and brainstem (IC12).

In addition to the spatial connectivity maps, ICA also produces an overall temporal fluctuation for each spatial network, that is, the time courses. We calculated correlation between the time courses from each pair of IC as the measure of between-network connectivity. As a preliminary effort to compare the inter-network connectivity, we performed a two-sample *t*-test on the Fisher-transformed between-network correlation values from the AgCC and control groups. We observe that the correlation value between IC5 (a bilateral parietal network) and IC14(a bilateral frontotemporal network) shows a significant difference ($p < 0.05$) between the AgCC and the control groups. Given the importance as well as the complexity on the inter-network connectivity, the interpretation of this preliminary observation requires more in-depth inter-network analysis in future work.

Seed region correlation analysis of resting-state fMRI

A two-sample *t*-test was performed on the intra-ROI functional connectivity and the IFC measures to study group differences between AgCC and controls (Table 1). The inferior PCC network (IC14) and the insular-opercular network (IC21) show significant decreases of both the intra-network connectivity and the IFC in AgCC ($p < 0.05$), with a strong trend toward lower intra-ROI functional connectivity of the precuneus-PCC network (IC18) encompassing both left and right hemispheres in the AgCC group ($p = 0.06$). IFC could not be calculated for the left frontoparietal network or the right frontoparietal network, as these IC spatial maps are almost entirely unilateral. However, intra-ROI functional connectivity within their respective hemispheres is significantly

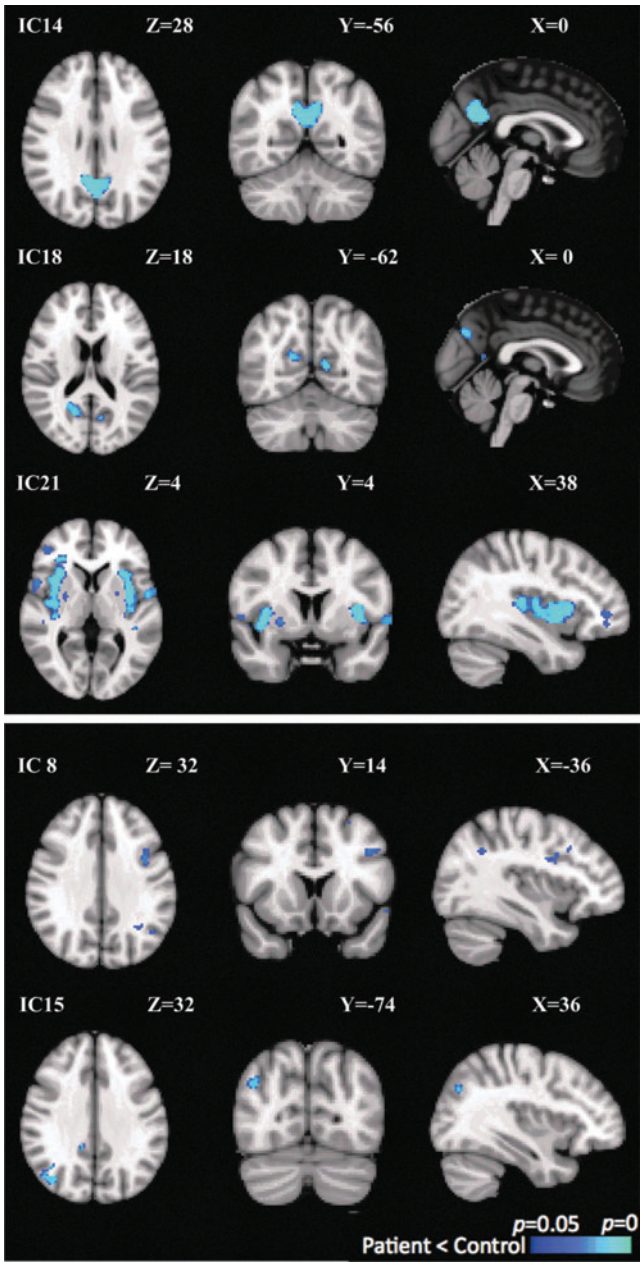

FIG. 5. Five resting-state networks containing regions of significantly reduced functional connectivity in AgCC versus controls: insular-opercular (IC21), posterior cingulate (IC14), precuneus/posterior cingulated (IC18), right frontoparietal network (IC15), and left frontoparietal network (IC8). For each component, the voxelwise two sample permutation test result is thresholded at a family-wise error rate of $p < 0.05$.

decreased in the AgCC group compared with controls in both networks ($p < 0.05$).

Connectomic analysis of resting-state fMRI

The mean weighted and group-level binary adjacency matrices are shown in Figure 6 for the control and AgCC groups. Qualitatively, both the weighted and binary matrices appear to be similar between groups. Notably, the homotopic interhemispheric connections present in the controls are also easily distinguished in the AgCC cohort (the diagonal of the bottom left and top right quarter of the matrices). The correlation coefficient between the weighted matrices is 0.78, and the edge agreement between the binary matrices is 0.91. The modular decompositions of the binary adjacency matrices are presented in Figure 7. The various modules are denoted by color, and only the edges between nodes in the same module (intramodular edges) are plotted. For the controls, five modules were detected that are similar to those detected in He and colleagues (2009) and are reminiscent of resting-state networks assessed with ICA (in this paper) and in Lee and colleagues (2012) and Jones and colleagues (2012). Generally, these modules break down into the following: bilateral frontal-posterior cingulate-occipital (Module 1), bilateral posterior parietal-inferior temporal (Module 2), bilateral occipital-inferior temporal (Module 3), bilateral temporal-parietal (Module 4), and subcortical-insular (Module 5). The modularity of this decomposition was 0.626. While there are some differences in the modules for the AgCC cohort (modularity of 0.612), they demonstrate that there is no drastic reorganization of the functional connectome in AgCC. The default mode network appears to be intact (Module 5), and the general topology of the subnetworks is the same. The Hubert Rand index (HRI) (Hubert and Baker, 1977), a measure of the similarity between two modular decompositions, is 0.735. We found the module decomposition on the individual level to be noisy and not a stable means to assess group differences. This observation is supported by the results of Jones and colleagues (2012), where the modular organization seemed to vary across individuals and across different time windows.

The statistical comparison of the intramodular edge strengths yielded five edges that have increased strength in AgCC compared with the controls. These edges were extracted using the modules defined from the AgCC group-binarized matrix. No additional edges were detected in the modules defined by the controls. These edges connect (1) inferior temporal (ITP) and right angular (ANG), (2) left precuneus (PCN) and right superior occipital (SOC), (3) left PCN and left middle occipital (MOC), (4) right PCN and left lingual (LIN), and (5) right PCN and left MOC. Unlike the ICA analysis, we did not find edges with decreased coupling using this analysis technique. However, using the regions implicated in the ICA analysis (Supplementary Table S1; Supplementary Data are available online at www.liebertpub.com/brain), we were able to detect decreased coupling between some of these regions ($p < 0.05$). These regions included (1) left and right rolandic operculum (ROP), (2) right ROP and right insula (INS), (3) left inferior frontal, occipital part (IFO), and (4) left ANG, and left IFO and right MOC. Just under the cutoff ($p < 0.06$), there are two additional edges connecting (1) left and right INS and (2) right posterior cingulate (PCC) and right PCN.

In Figure 8, we present the global graph metrics as a function of density for both the control (green) and the AgCC (red) groups. There are no significant differences for any of the metrics, at any density, providing further evidence that there is no pervasive cortical or subcortical reorganization of the functional connectome in patients with AgCC. The global graph metrics and the modular decomposition measure coarse properties of a network. Therefore, to assess the networks at a finer scale, we employed edge-space similarity

Table 1. Intra-Regional and Interhemispheric Functional Connectivity from Seed Region Correlation Analysis, Using ROIs Defined by the Voxel-Wise Two-Sample *t*-Test on Independent Components with $p < 0.05$ from ICA

	Controls (mean ± std. dev.)	*AgCC (mean ± std. dev.)*	p-*Value*
Insular-opercular			
Intra-ROI (L + R)	0.13 ± 0.06	0.08 ± 0.04	**0.04**
Intra-ROI (L only)	0.15 ± 0.08	0.11 ± 0.06	0.22
Intra-ROI (R only)	0.13 ± 0.05	0.09 ± 0.05	0.09
Interhemispheric (L-ROI vs. R-ROI)	0.88 ± 0.06	0.55 ± 0.27	**< 0.01**
Posterior cingulated cortex (PCC)			
Intra-ROI (L + R)	0.44 ± 0.12	0.25 ± 0.08	**< 0.01**
Intra-ROI (L only)	0.49 ± 0.10	0.31 ± 0.13	**< 0.01**
Intra-ROI (R only)	0.42 ± 0.15	0.26 ± 0.11	**0.01**
Interhemispheric (L-ROI vs. R-ROI)	0.87 ± 0.07	0.78 ± 0.13	0.06
Precuneus/PCC			
Intra-ROI (L + R)	0.27 ± 0.13	0.18 ± 0.11	0.07
Intra-ROI (L only)	0.33 ± 0.12	0.25 ± 0.11	0.11
Intra-ROI (R only)	0.26 ± 0.13	0.17 ± 0.12	0.11
Interhemispheric (L-ROI vs. R-ROI)	0.80 ± 0.11	0.68 ± 0.24	0.28
Left frontoparietal			
Intra-ROI (L only)	0.15 ± 0.06	0.05 ± 0.04	**< 0.01**
Right frontoparietal			
Intra-ROI (R only)	0.32 ± 0.13	0.25 ± 0.11	0.16

The intra-ROI (both hemispheres combined, left hemisphere only, and right hemisphere only) connectivity was measured by the average pairwise voxel-based correlation within each ROI. The interhemispheric functional connectivity was measured by the correlation between the mean time series within separate ROIs in the left versus right hemisphere. For predominantly unilateral independent components, only intra-ROI functional connectivity from the hemisphere containing the resting-state network is shown. Statistical significance ($p < 0.05$) is noted in bold.

ROI, regions of interest; ICA, independent component analysis.

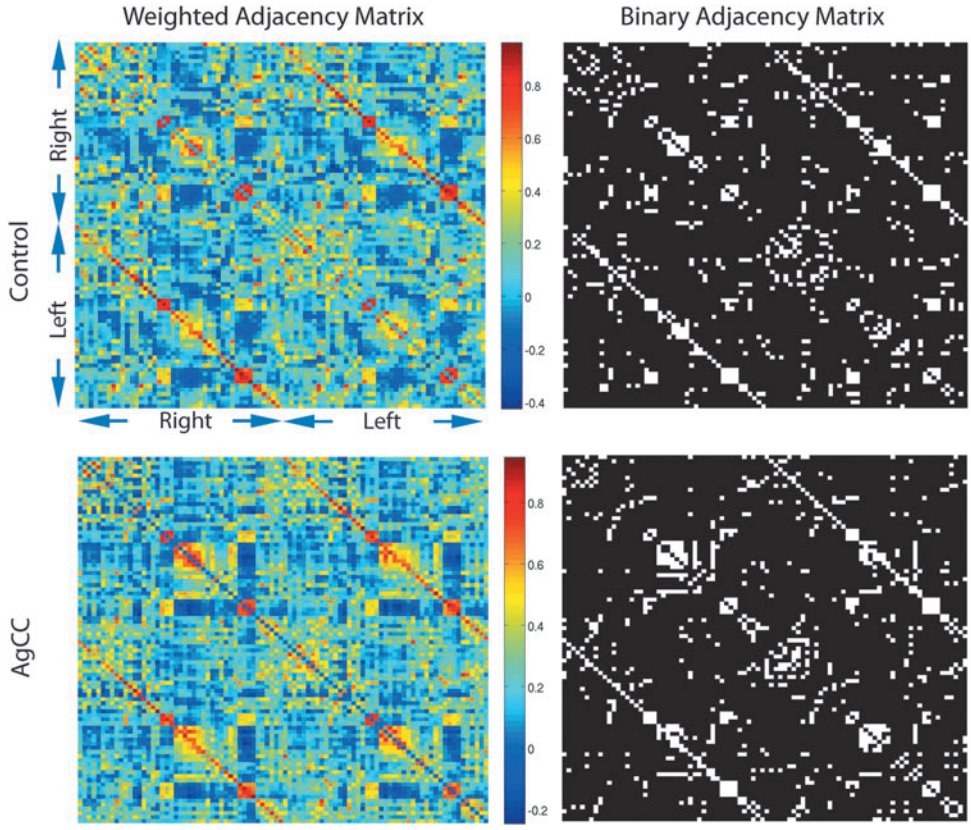

FIG. 6. The mean weighted adjacency matrix and the group-binarized adjacency matrix for the controls and AgCC. As depicted, all the right brain regions are in the first 45 rows/columns. Qualitatively, these matrices are similar, the edge similarity of the weighted matrices is 0.78, and the binary edge agreement between the binary matrices is 0.91.

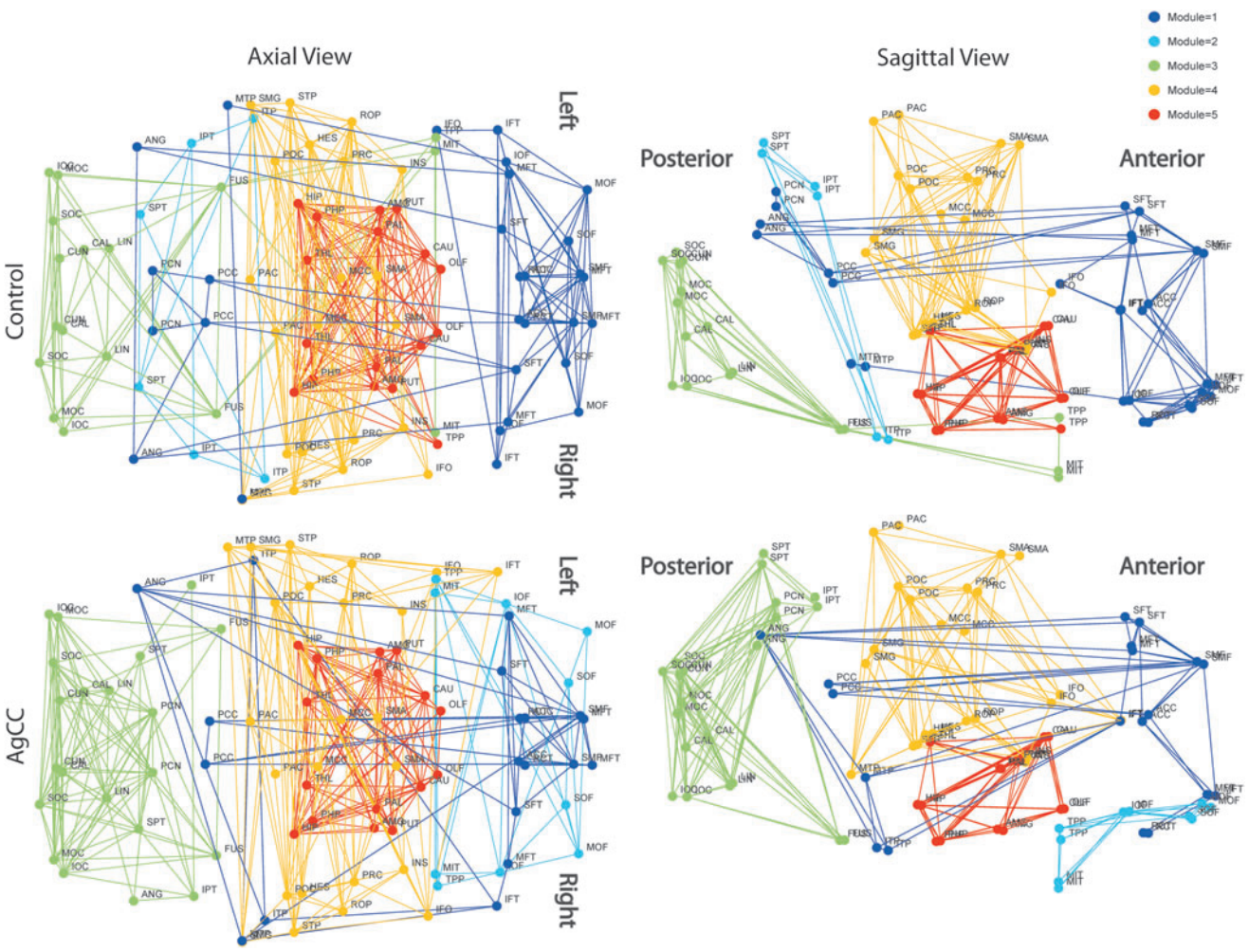

FIG. 7. The modular decomposition of the group-binarized matrix for the controls and AgCC in both axial and sagittal views. There are five modules detected in both groups, Modules 1–3 and 5 are topologically similar, while Module 4 in both groups is different and relatively small. The Hubert Rand index (HRI), a measure of the similarity between two modular decompositions, is 0.735.

calculations. At this higher level of granularity, we find group differences as presented in Table 2. All the groupings of the edges of both the weighted and binarized connectomes indicate that AgCC subjects have significantly higher group variations in their edges than the control group. Since we make a distinction between the consistency of the right and left intrahemispheric connections, we wanted to confirm that increased variability in AgCC is not due to the fact that they are equally split between right- and left-handed individuals, whereas all the controls are right-handed. In Supplementary Table S2, we provide the same analysis with only the right-handed individuals (11 controls versus 6 right-handed AgCC) and only the left-handed individuals (11 controls versus 5 left-handed AgCC). For the most part, this analysis supports the assumption that our results in Table 2 are not entirely contingent on the mixture of handedness in the AgCC group. The exceptions are (1) the weighted left intrahemispheric connections for the right-handed AgCC are not significantly more variable than for the controls and (2) the binary right intrahemispheric connections for the left-handed AgCC are not significantly more variable than for the controls.

Voxel-based morphometry of structural MRI

The VBM results of AgCC versus controls show that the significant anatomical differences are in the white matter adjacent to the atria and trigones of both lateral ventricles, where the intensity in the AgCC group was less than that of controls (Figure 9). This reflects the well-known "colpocephaly" from expansion of the posterior aspects of the lateral ventricles due to reduced volume of the periventricular white matter that is almost universally seen in AgCC (Hetts *et al.*, 2006). In addition, the four partial AgCC cases are included in the AgCC group, as shown in Figure 1, which may contribute to the missing difference at the body of the corpus callosum in the VBM results.

There were no regions in which the brain parenchymal intensity in the AgCC group exceeded that of the control group. No significant anatomic differences between AgCC and controls were found in regions showing significant functional connectivity differences. Therefore, the functional connectivity differences shown by both ICA and seed region correlation analysis at the precuneus, PCC and insular-opercular regions are not likely to be artifactual differences introduced

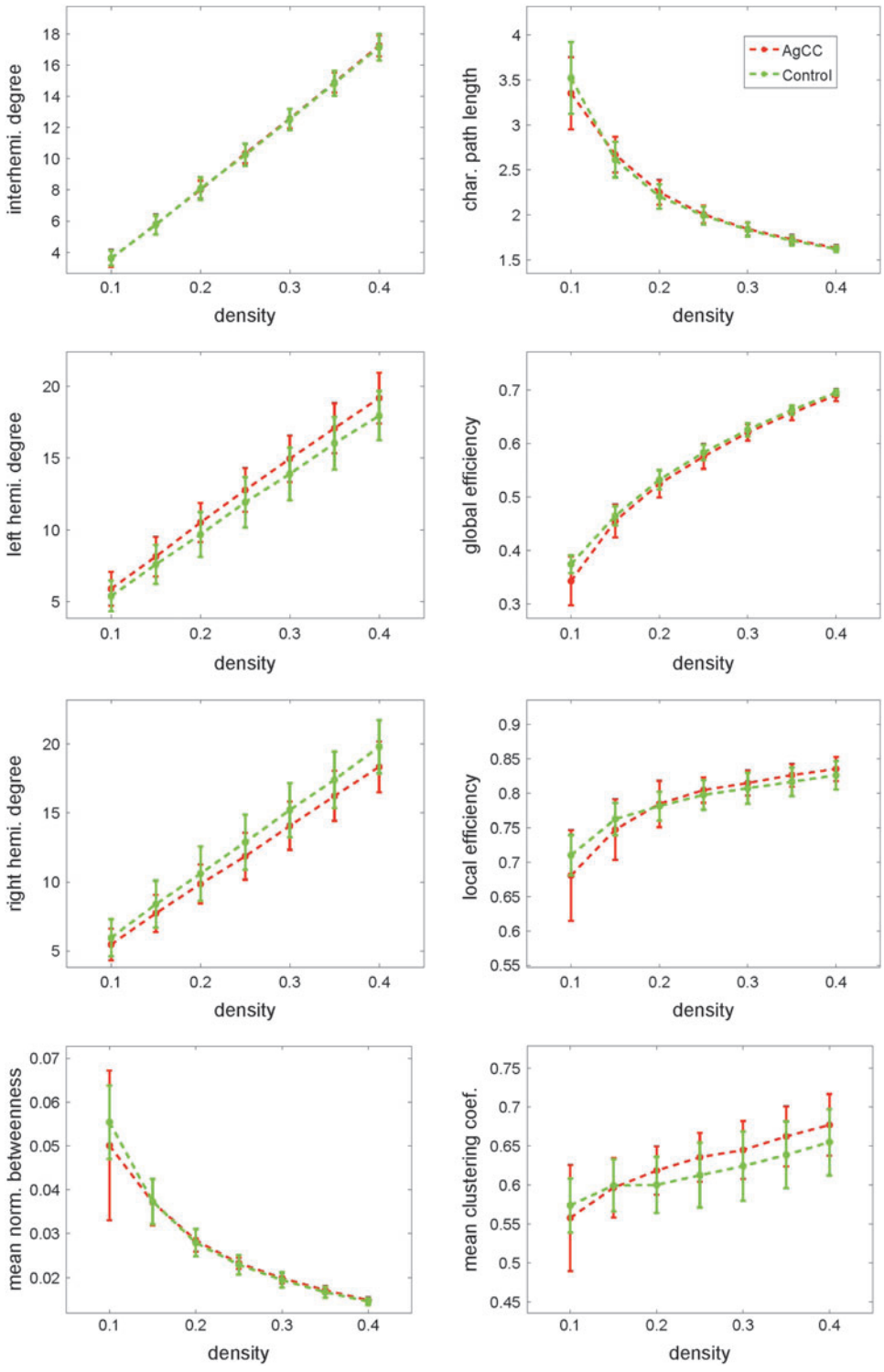

FIG. 8. Mean summary graph metrics for the control (green) and AgCC (red) connectomes binarized at various density levels (0.1 to 0.4). The standard deviation is plotted as an error bar. There were no statistically significant differences between groups at any density level, for any of the metrics computed.

by structural anomalies in AgCC through the image registration process.

Effect of co-morbid brain malformations associated with AgCC

The majority of individuals with callosal dysgenesis have additional brain malformations, which are most commonly gray matter heterotopias and abnormal sulcation (Hetts *et al.*, 2006). Six of the 11 AgCC subjects in our cohort had co-morbid heterotopias and/or sulcal abnormalities. To exclude this potential confounding factor, the subgroup of six AgCC patients without other associated malformations and six age- and IQ-matched controls were selected for a *post hoc* seed region correlation analysis. Due to the smaller sample size, the results were less significant than the full analysis

Table 2. Edges in AgCC Group with Statistically Increased or Decreased Coupling Strengths Between ROI#1 and ROI#2 as Compared with the Controls

AgCC defined modules				
ROI #1	*ROI #2*	*Controls*	*AgCC*	p-*Value*
R-ITP	R-ANG	0.11 ± 0.12	0.54 ± 0.23	0.0002
L-PCN	R-SOC	0.12 ± 0.15	0.50 ± 0.22	0.0007
L-PCN	L-MOC	0.18 ± 0.21	0.54 ± 0.17	0.0002
R-PCN	L-LIN	0.16 ± 0.20	0.54 ± 0.18	0.0003
R-PCN	L-MOC	0.12 ± 0.15	0.48 ± 0.20	0.0002

The edges were extracted from the modules (as defined by the AgCC modular partition) and all intramodular edges were included in the analysis. The p-values were FDR corrected, and only those surviving correction are provided. These edges involve inferior temporal (ITP), angular (ANG), precuneus (PCN), superior occipital (SOC), middle occipital (MOC), and lingual (LIN). There were no additional connections in the analysis using the control-defined modules. The mean and standard deviation is provided for the control and AgCC groups.

AgCC, agenesis of the corpus callosum.

on all 22 subjects but significantly decreased interhemispheric connectivity was still observed for the insular-opercular (AgCC: 0.66 ± 0.21; controls: 0.90 ± 0.04) and PCC (AgCC: 0.60 ± 0.20; controls: 0.82 ± 0.08) regions ($p < 0.05$). The subgroup difference of IFC in the precuneus/PCC was, however, not significant (AgCC: 0.79 ± 0.15; controls: 0.74 ± 0.10; $p = 0.48$).

Effect of complete versus partial AgCC

In order to address whether there are different effects of complete versus partial AgCC on brain functional connectivity, we performed a *post hoc* analysis. Due to the small sample size, we did not perform a separate group ICA analysis for the complete and partial AgCC subjects and matched normal controls. Instead, we performed a *post hoc* seed region correlation analysis between the subgroup of the seven complete AgCC (cAgCC) subjects with seven matched controls on the five networks with decreased functional connectivity in AgCC identified in the full 22 subject analysis (Fig. 2). The results show a similar result of decreased IFC in the insula-opercula (cAgCC: 0.58 ± 0.21; controls: 0.89 ± 0.04; $p < 0.05$) with a strong trend in the PCC (cAgCC: 0.69 ± 0.15; controls: 0.81 ± 0.07; $p = 0.06$). However, the reduced IFC in the precuneus/PCC was less significant (cAgCC: 0.68 ± 0.22; controls: 0.77 ± 0.10; $p = 0.31$).

We also apply the connectomic analysis to the cAgCC subgroup. The adjacency matrices and modular decomposition for the cAgCC are shown in Supplementary Figure S1. Qualitatively, the group weighted and binary adjacency matrices and modular decomposition of the cAgCC is similar to the results from the controls and AgCC in Figures 6 and 7. Homotopic interhemispheric connections are present in the cAgCC despite the complete absence of the corpus callosum. The module decomposition in cAgCC (modularity of 0.580) has a similar topology to the four major modules (Modules 1–3 and 5) in the control and AgCC groups. A quantitative analysis of the similarity yields a weighted edge consistency between the controls and cAgCC of 0.720 and between the AgCC and cAgCC of 0.947. The binary edge consistency between the controls and cAgCC is 0.906 and between AgCC and cAgCC is 0.947. The HRI between the modular partition of the controls and cAgCC is 0.366 and between AgCC and cAgCC is 0.381. This denotes that, while the qualitative organization of the modules seems to be very similar for the cAgCC subgroup as for the control and overall AgCC groups, there are subtle differences and one of the fewer modules that result in this relatively low HRI. We also repeated the edge-space correlation analysis for cAgCC alone, with the results shown in Supplementary Table S2. We found that all groupings of edges for both the weighted and binary are significantly more variable for the cAgCC subgroup.

Discussion

Callosal connectivity and resting-state functional networks

In the case of fMRI, functional connectivity refers to temporal correlations of the BOLD signal of spatially disparate cortical regions, which can be measured using univariate hypothesis-driven methods such as seed region correlation analysis (Biswal *et al.*, 1995) or multivariate data-driven techniques such as ICA (Beckmann and Smith, 2004; Calhoun *et al.*, 2001; Kiviniemi *et al.*, 2003; McKeown *et al.*, 1998) and functional connectomics (Bullmore and Sporns, 2009; Sporns *et al.*, 2005; Wang *et al.*, 2010). ICA is typically employed to decompose the sequential volumes of fMRI data into a set of relatively uncorrelated spatial maps, each with sparse and localized foci, and a set of time courses summarizing the temporal fluctuations of each spatial map. Functional connectomics apply graph theoretic techniques to whole-brain functional networks to reveal differences in network topology. Both ICA and functional connectomics identify functional connectivity patterns throughout the entire brain and do not require any prior knowledge of the location of

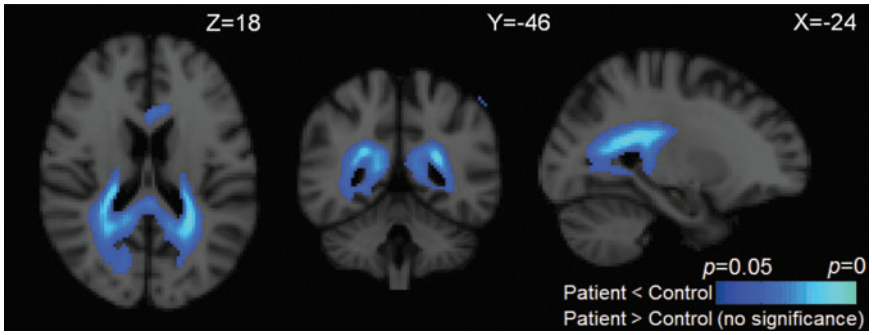

FIG. 9. Voxel-based morphometry shows decreased T1-weighted contrast of posterior periventricular white matter in AgCC patients compared with controls.

functionally affected areas. Therefore, a broad range of brain regions can be examined to determine the effect of callosal connectivity. We found that the qualitative organization of 17 resting-state networks calculated with ICA and five functional modules extracted from the connectome, most of which are bilateral, did not differ qualitatively between the AgCC group and the controls. In subjects with complete AgCC, this could be explained by interhemispheric communication achieved through alternate pathways such as the anterior commissure and subcortical commissural connections. Indeed, a prior structural MR imaging study of AgCC showed that the anterior commissure is enlarged in 10% of subjects with AgCC (Hetts *et al.*, 2006). Neuropsychological testing has suggested that a larger anterior commissure is associated with better cognition in AgCC (Barr and Corballis, 2002).

The recruitment of indirect commissural routes in place of direct callosal avenues between the hemispheres should result in reduced interhemispheric functional connectivity, as polysynaptic pathways would be required for communication instead of monosynaptic ones. This hypothesis is supported by our quantitative measurements of IFC in AgCC, which show significant reductions in three of the most highly interconnected cortical regions: the precuneus, the posterior cingulate, and the insula-opercula. These bilateral cortical hubs would be expected to be more affected by the absence of direct callosal routes than less highly connected areas of the cerebral cortex.

An alternative, but not mutually exclusive, explanation for the findings is that a common external driving force, specifically the thalamus, is preserving the bilateral functional connectivity in AgCC. This could explain why we did not find reduced interhemispheric functional connectivity in primary sensory areas, which receive direct inputs from the thalamus. Rather, the differences in interhemispheric connectivity were observed in association cortical areas further downstream from the primary sensory areas. It may be that bilateral temporal synchrony is lost the further away information travels from cortical areas receiving direct sensory drive from the thalamus. The potential of the thalamus to coordinate activity across the two hemispheres can also be seen in cases of complete commisurotomy, as discussed in the next section.

It is possible that additional bilateral resting-state networks also have reduced functional connectivity in AgCC, but not of great enough magnitude to be detectable by whole-brain ICA or functional connectomics at the sample size of our study. In addition, at the low temporal resolution of fMRI (2 sec per brain volume in this study), it is not possible to differentiate neural information transmission via single versus multiple synaptic pathways. In an magnetoencephalography (MEG) resting-state connectivity study of partial and complete AgCC patients (Hinkley *et al.*, 2012), both inter- and intra-hemispheric connectivity was diminished in the alpha-band (8–12 Hz) in frontal, parietal, and occipital regions in AgCC. MEG has a temporal resolution in the order of a millisecond and is exceedingly more sensitive to discrepancies in timing than fMRI.

Relationship of present work to prior resting-state fMRI studies of callosal connectivity

In healthy controls, there is evidence that intrahemispheric correlations tend to be positive, while the same heterotopic interhemispheric correlations tend to be negative (Gee *et al.*, 2011). In a complementary study in which homotopic interhemispheric connections were assessed in healthy controls (Stark *et al.*, 2008), the correlations were strongest between primary sensory areas and weakest between areas involved in heteromodal association. While studies of interhemispheric connectivity in healthy controls indirectly assess the role of the corpus callosum in coordinating neural activity between the two hemispheres, these studies cannot differentiate callosal connectivity from interhemispheric connectivity due to other sources such as alternate commissural routes or common thalamic drive.

To date, there has been little published literature on the effect of impaired or absent callosal connectivity on resting-state networks using BOLD fMRI. In a case report of a 6-year-old child imaged before and after callosotomy performed for intractable seizures, interhemispheric functional connectivity measured using seed region correlations was found to be greatly reduced postoperatively, but they found preserved intrahemispheric functional connectivity (Johnston *et al.*, 2008). In a similar case report, Uddin and colleagues (2008) characterized bilateral functional networks extracted with ICA in a subject with a complete commisurotomy. The preservation of functional connectivity across the cerebral hemispheres without any commissural tracts, including the corpus callosum, suggests that subcortical areas can coordinate synchrony between bilateral cortical regions. Quigley and colleagues (2003) studied three subjects with AgCC using seed region correlations and found reduced interhemispheric functional connectivity of sensorimotor cortex and auditory cortex compared with a normal volunteer. In Lowe and colleagues (2008), the structural and functional connectivity of the right and left sensorimotor cortex was computed using resting-state fMRI and diffusion tractography in patients with multiple sclerosis (MS) and healthy controls. They found a significant correlation between tract integrity and degree of functional connectivity in both the controls and MS patients, although they did not find reduced functional connectivity in the MS patients. These prior studies of callosal connectivity on BOLD fMRI temporal correlations have been limited by very small numbers of subjects, narrow selection of brain regions examined, or lack of multivariate analysis techniques.

Most similar to the current study is a recent investigation of functional connectivity in eight complete AgCC patients showing that the ICA-based resting-state networks were qualitatively intact (Tyszka *et al.*, 2011), in agreement with our qualitative results (Fig. 4). However, this prior report did not include an evaluation of voxel-wise quantitative differences in functional connectivity between AgCC and controls that could be compared with the results presented in Figure 5 and Tables 1–3.

Relationship between functional and structural connectivity in AgCC

Many studies comparing resting-state fMRI and diffusion MRI measures of functional and structural connectivity, respectively, in normal volunteers show that they are highly correlated (Damoiseaux and Greicius, 2009; Greicius *et al.*, 2009; Honey *et al.*, 2009, 2010, Skudlarski *et al.*, 2008). Recent comparisons of structural and functional connectivity in the

Table 3. Edge-Space Similarity Results, the Pair-Wise Weighted and Binary Similarity Was Computed for All Individuals in the Controls and AgCC Group

	Controls	*AgCC*	p-*Value*
Weighted all connections	0.40 ± 0.09	0.30 ± 0.07	7.4E-09
Weighted interhemi.	0.41 ± 0.10	0.29 ± 0.08	3.6E-19
Weighted intrahemi.	0.39 ± 0.08	0.31 ± 0.07	9.1E-13
Weighted intrahemi. (right)	0.41 ± 0.08	0.31 ± 0.08	5.7E-18
Weighted intrahemi. (left)	0.37 ± 0.10	0.31 ± 0.08	1.6E-06
Binary all connections	0.77 ± 0.02	0.74 ± 0.02	2.0E-07
Binary interhemi.	0.77 ± 0.02	0.74 ± 0.02	3.8E-20
Binary intrahemi.	0.76 ± 0.02	0.74 ± 0.02	4.8E-07
Binary intrahemi. (right)	0.77 ± 0.02	0.75 ± 0.02	9.5E-10
Binary intrahemi. (left)	0.74 ± 0.04	0.73 ± 0.03	0.003

The mean, standard deviation, and *p*-values are provided.

normal human brain using diffusion tractography and resting-state fMRI show that direct anatomic connections imply functional connectivity, but functional connectivity does not guarantee direct anatomic connections (Honey *et al.*, 2009, 2010). This asymmetry is thought to reflect functional connectivity that arises from indirect polysynaptic pathways or a common external driving force.

In a recent paper (Owen *et al.*, 2013a), the structural connectome of complete AgCC subjects was investigated using diffusion MRI and tractography. This work found that the modular organization in cAgCC is profoundly reorganized. Most notably, the "structural core," a bilateral anterior-posterior module that overlaps the default-mode network, was broken up into separate anterior and posterior segments in each cerebral hemisphere. In addition, the topology of the intrahemispheric modules also differed between the controls and AgCC. Finally, the organization of the structural connectome was more variable among individuals with AgCC than among normal controls, both at the modular level and at the level of edge space similarity. Hypothesis-driven analyses of structural connectivity of partial AgCC using fiber tractography (Tovar-Moll *et al.*, 2007; Wahl *et al.*, 2009) have shown that some of these individuals have novel heterotopic callosal connections such as sigmoid bundles not seen in the control population. These patterns of connectivity were not seen in all pAgCC subjects, which implies that the aberrant anatomic connectivity of AgCC is individualized, thereby contributing to the relatively variable topology observed across subjects in their structural connectomes (Owen *et al.*, 2013a). The inconsistent organization of the structural connectome in AgCC could provide a basis for the larger inter-subject variation that we observe in the functional connectivity of these subjects versus normal volunteers (Tables 3 and Supplementary Table S2).

Functional specialization of the insula

It has been recently demonstrated that the insula can be partitioned into two or three subregions with different functional networks that are associated with each subregion (Cauda *et al.*, 2011, Deen *et al.*, 2010). In light of the functional specialization of the insula, diminished connectivity in the anterior insula from the ICA analysis may indicate that AgCC has a significant effect on the anterior insular network, including the anterior cingulate cortex, middle/inferior frontal cortex, temporoparietal network, and their related functions, that is, emotional salience and attentional control. Individuals with AgCC are known to have diminished pain sensitivity and altered emotional processing (Moes *et al.*, 2009). This corresponds with the insula's prominent role as a center of the "pain network," particularly as a convergence zone for the affective and sensory components of pain (Augustine 1996; Vanhaudenhuyse *et al.*, 2009).

Functional connectivity of unilateral networks in AgCC

Weak reductions in functional connectivity of AgCC versus controls were identified in predominantly unilateral frontoparietal networks of both the left and right hemispheres using ICA, demonstrating that altered resting-state BOLD activity in AgCC is not completely limited to interhemispheric connectivity. AgCC is thought to result from aberrant axonal guidance during fetal development, and alterations in white matter can be seen in this disorder beyond partial or complete absence of the corpus callosum; for example, the reduced posterior periventricular white matter volume that results in colpocephaly (Paul *et al.*, 2007) and also reduced volume and microstructural integrity of the ventral cingulum bundle (Nakata *et al.*, 2009). While AgCC is best recognized for its lack of connections, there are clear, novel connections not seen in healthy controls, such as Probst bundles and sigmoid bundles. As previously discussed, the results in Tovar-Moll and associates (2007) and Wahl and associates (2009) suggest that patients with AgCC could be focally hyperconnected. This hypothesis is supported by the increased functional connectivity between the precuneus and occipital-parietal regions (Table 2) in AgCC versus controls. In addition, the increased variability of functional connectivity among AgCC individuals compared with that among controls (Table 3) further suggests that the polysynaptic rerouting could differ from person to person. This agrees with the results of Owen and associates (2013a) that the structural connectome was also more variable among cAgCC subjects relative to the controls and that the mean degree of the AgCC structural networks was not significantly reduced compared with the controls. Therefore, greater variability of the structural connectome likely represents a major basis for the abnormally high intersubject variation in the functional connectome observed in AgCC.

Study limitations and future directions

Our sample size of 11 AgCC subjects is small and limits the magnitude of differences we can detect between the controls and AgCC. In the future, we plan to expand our AgCC cohort for adequate statistical power in correlating measures of structural and functional connectivity with behavioral measures. Including partial AgCC subjects in the present study has increased statistical power, but also presents a confound. While we have demonstrated that the results are not driven by the partial or the complete AgCC subgroups alone, with more subjects in the future, we will be able to more fully analyze functional connectivity across the entire spectrum of callosal dysgenesis from complete absence to only mild hypogenesis. The number of left-handed AgCC participants presented a challenge in control recruitment. Given the age, gender, and IQ constraints, we were not able to match for handedness. Wherever applicable, as with the

partial AgCC subjects, we have attempted to examine the effect of handedness.

For the connectomic analysis, we have used 90 cortical and subcortical regions from the AAL atlas. These regions are fairly large, and averaging over them might obscure group differences detected in the ICA analysis. In addition, although the preprocessing pipeline employed here was based on other pipelines in the literature, we acknowledge that the choice of preprocessing steps can have an effect on the data and results (Gotts *et al.*, 2013; Saad *et al.*, 2012; Van Dijk *et al.*, 2010).

AgCC is a useful model for the study of the relation between structural and functional connectivity. We plan to combine structural connection information from fiber tractography with the functional coupling from both fMRI and MEG resting-state measurements. With this multimodal data, we should be able to shed light on the mechanism that preserves functional connectivity in subjects with such profoundly altered structural connectivity. Similarly, the role of the Probst bundles in the transmission of information in the AgCC brain is not well understood. We plan to explore changes in functional connectivity that can be attributed to the presence of the Probst bundles in our future work. One possible way to target the effect of Probst bundles would be to use regional homogeneity (ReHo) methods to compare the internal synchrony of the cortical regions that make connections using the Probst bundles.

Conclusion

Despite the loss of callosal connectivity in AgCC, the qualitative organization of 17 resting-state cortical networks and five modules extracted from the functional connectome, most of which are bi-hemispheric, was the same in the AgCC group as in matched normal controls. However, quantitative measurements of intra-network functional connectivity and/or interhemispheric functional connectivity were significantly reduced in AgCC for 5 of the 17 networks. Two of the three bilateral cortical networks with significantly reduced connectivity localized to the precuneus and the posterior cingulate, which are the two most highly interconnected regions of the cerebral cortex and constitute the hubs of the default mode network (Hagmann *et al.*, 2008). The third was the bilateral insular-opercular network, also cortical hubs. This network demonstrated the strongest decrease in functional connectivity in AgCC subjects, which may help explain the diminished pain sensitivity and altered emotional processing commonly found in acallosal individuals. Overall, the findings may result from indirect commissural pathways maintaining bilateral resting-state networks in the absence of direct callosal routes, although with reduced interhemispheric functional connectivity in highly connected hub regions, and possibly also a mechanism involving a common external impetus such as the thalamus enforcing bihemispheric temporal synchrony. The strength of inter-regional functional connectivity was also strikingly more variable across AgCC subjects than controls, which may in part reflect the less consistent organization of their anatomic connectivity, as shown in a recent study of the AgCC structural connectome (Owen *et al.*, 2013a). These initial observations demonstrate the great potential of resting-state fMRI to reveal abnormal function in the malformed brain and thereby also help elucidate the function of the normal human brain.

Acknowledgments

This study was supported by a grant from the American Society of Neuroradiology, the UCSF Program in Breakthrough Biomedical Research and Award Numbers R01 NS060776, R01 EB009756, and R01 HD072074 of the U.S. National Institutes of Health (NIH). The content is solely the responsibility of the authors and does not necessarily represent the official views of the NIH. The authors would like to thank J. Michael Tyszka, Lynn Paul, Warren Brown, and Ralph Adolphs for helpful discussions.

Author Disclosure Statement

No competing financial interests exist.

References

Aboitiz F, Scheibel AB, Fisher RS, Zaidel E. 1992. Fiber composition of the human corpus callosum. Brain Res 598: 143–153.

Abou-Elseoud A, Starck T, Remes J, Nikkinen J, Tervonen O, Kiviniemi V. 2010. The effect of model order selection in group PICA. Hum Brain Mapp 31:1207–1216.

Augustine JR. 1996. Circuitry and functional aspects of the insular lobe in primates including humans. Brain Res Brain Res Rev 22:229–244.

Barr MS, Corballis MC. 2002. The role of the anterior commissure in callosal agenesis. Neuropsychology 16:459–471.

Basser PJ, Pajevic S, Pierpaoli C, Duda J, Aldroubi A. 2000. *In vivo* fiber tractography using DT-MRI data. Magn Reson Med 44:625–632.

Bassett D, Brown J, Deshpande V, Carlson J, Grafton S. 2011. Conserved and variable architecture of human white matter connectivity. Neuroimage 54:1262–79.

Beckmann CF, Smith SM. 2004. Probabilistic independent component analysis for functional magnetic resonance imaging. IEEE Trans Med Imaging 23:137–152.

Bell AJ, Sejnowski TJ. 1995. An information maximisation approach to blind separation and blind deconvolution. Neural Comput 7:1129–1159.

Biswal B, Yetkin FZ, Haughton VM, Hyde JS. 1995. Functional connectivity in the motor cortex of resting human brain using echo-planar MRI. Magn Reson Med 34:537–541.

Blondel V, Guillame JL, Lambiotte R, Lefebvre E. 2008. Fast unfolding of communities in large networks. J Stat Mech 2008:P10008.

Bullmore E, Sporns O. 2009. Complex brain networks: graph theoretical analysis of structural and functional systems. Nat Rev Neurosci 10:186–198.

Calhoun VD, Adali T, Pearlson GD, Pekar JJ. 2001. A method for making group inferences from functional MRI data using independent component analysis. Human Brain Mapping 14:140–151.

Cauda F, D'Agata F, Sacco K, Duca S, Geminiani G, Vercelli A. 2011. Functional connectivity of the insula in the resting brain. Neuroimage 55:8–23.

Damoiseaux JS, Rombouts SA, Barkhof F, Scheltens P, Stam CJ, Smith SM, Beckmann CF. 2006. Consistent resting-state networks across healthy subjects. Proc Natl Acad Sci U S A 103:13848–13853.

Damoiseaux JS, Greicius MD. 2009. Greater than the sum of its parts: a review of studies combining structural connectivity and resting-state functional connectivity. Brain Struct Funct 213:525–533.

Deen B, Pitskel NB, Pelphrey KA. 2010. Three systems of insular functional connectivity identified with cluster analysis. Cereb Cortex 21:1498–1506.

Erhardt E, Rachakonda S, Bedrick E, Allen E, Adali T, Calhoun VD. 2010. Comparison of multi-subject ICA methods for analysis of fMRI data. Human Brain Mapp 32:2075–2095.

Gee DG, Biswal BB, Kelly C, Stark DE, Margulies DS, Shehzad Z, Uddin LQ, Klein DF, Banich MT, Castellanos FX, Milham MP. 2011. Low frequency fluctuations reveal integrated and segregated processing among the cerebral hemispheres. Neuroimage 54:517–527.

Gotts SJ, Saad ZS, Jo HJ, Wallace GL, Cox RW, Martin A. 2013. The perils of global signal regression for group comparisons: a case study of Autism Spectrum Disorders. Front Hum Neurosci 7:356.

Greicius MD, Krasnow B, Reiss AL, Menon V. 2003. Functional connectivity in the resting brain: a network analysis of the default mode hypothesis. Proc Natl Acad Sci USA 100: 253–258.

Greicius MD, Supekar K, Menon V, Dougherty RF. 2009. Resting-state functional connectivity reflects structural connectivity in the default mode network. Cereb Cortex 19:72–78.

Hagmann P, Cammoun L, Gigandet X, Meuli R, Honey CJ, Wedeen VJ, Sporns O. 2008. Mapping the structural core of human cerebral cortex. PLoS Biol 6:e159.

He Y, Wang J, Wang L, Chen ZJ, Yan C, *et al.* 2009. Uncovering Intrinsic Modular Organization of Spontaneous Brain Activity in Humans. PLoS One 4: e5226.

Hetts SW, Sherr EH, Chao S, Gobuty S, Barkovich AJ. 2006. Anomalies of the corpus callosum: an MR analysis of the phenotypic spectrum of associated malformations. AJR Am J Roentgenol 187:1343–1348.

Hinkley LBN, Marco EJ, Findlay AM, Honma S, Jeremy RJ, *et al.* 2012. The Role of Corpus Callosum Development in Functional Connectivity and Cognitive Processing. PLoS One 7: e39804.

Honey CJ, Sporns O, Cammoun L, Gigandet X, Thiran JP, Meuli R, Hagmann *P*. 2009. Predicting human resting-state functional connectivity from structural connectivity. Proc Natl Acad Sci U S A 106:2035–2040.

Honey CJ, Thivierge JP, Sporns O. 2010. Can structure predict function in the human brain? Neuroimage 52:766–776.

Hubert LJ, Baker FB. 1977. The comparison and fitting of given classification schemes. J Mathematical Psychology 16: 233–253.

Johnston JM, Vaishnavi SN, Smyth MD, Zhang D, He BJ, Zempel JM, Shimony JS, Snyder AZ, Raichle ME. 2008. Loss of resting interhemispheric functional connectivity after complete section of the corpus callosum. J Neurosci 28:6453–6458.

Jones DT, Vemuri P, Murphy MC, Gunter JL, Senjem ML, *et al.* 2012. Non-Stationarity in the "Resting Brain's" Modular Architecture. PLoS One 7: e39731.

Kiviniemi V, Kantola JH, Jauhiainen J, Hyvärinen A, Tervonen O. 2003. Independent component analysis of nondeterministic fMRI signal sources. Neuroimage 19:253–260.

Lee MH, Hacker CD, Snyder AZ, Corbetta M, Zhang D, *et al.* 2012. Clustering of Resting State Networks. PLoS One 7: e40370.

Li Y, Yang F, Shetty C, Venugopal S, Bukshpun P, Wakahiro M, Sherr E, Mukherjee P. 2011. Independent component analysis of resting-state fMRI reveals diminished functional connectivity in callosal dysgenesis [abstract]. ISMRM Proc. Intl. Soc. Mag. Reson. Med. 19.

Lowe MJ, Beall EB, Sakaie KE, Koenig KA, Stone L, Marrie RA, Phillips MD. 2008. Resting state sensorimotor functional connectivity in multiple sclerosis inversely correlates with transcallosal motor pathway transverse diffusivity. Hum Brain Mapp 29:818–827.

McKeown MJ, Makeig S, Brown GG, Jung TP, Kindermann SS, Bell AJ, Sejnowski TJ. 1998. Analysis of fMRI data by blind separation into independent spatial components. Hum Brain Mapp 6:160–188.

Meskaldji DE, Ottet M, Cammoun L, Hagmann P, Meuli R, Eliez S, Thiran JP, Morgenthaler S. 2011. Adaptive Strategy for the Statistical Analysis of Connectomes, PLoS One 6:e23009.

Moes P, Schilmoeller K, Schilmoeller G. 2009. Physical, motor, sensory and developmental features associated with agenesis of the corpus callosum. Child Care Health Dev 35:656–672.

Nakata Y, Barkovich AJ, Wahl M, Strominger Z, Jeremy RJ, Wakahiro M, Mukherjee P, Sherr EH. 2009. Diffusion abnormalities and reduced volume of the ventral cingulum bundle in agenesis of the corpus callosum: A 3T imaging study. AJNR Am J Neuroradiol 30:1142–1148.

Owen JP, Li YO, Ziv E, Strominger Z, Gold J, Bukhpun P, Wakahiro M, Friedman EJ, Sherr EH, Mukherjee *P*. 2013a. The structural connectome of the human brain in agenesis of the corpus callosum. Neuroimage 70:340–355.

Owen JP, Ziv E, Bukshpun P, Pojman N, Wakahiro M, Berman J, Roberts TP, Friedman EJ, Sherr EH, Mukherjee *P*. 2013b. Test-Retest Reliability of Computational Network Measurements Derived from the Structural Connectome of the Human Brain. Brain Connect 3:160–176.

Paul LK, Brown WS, Adolphs R, Tyszka JM, Richards LJ, Mukherjee P, Sherr EH. 2007. Agenesis of the corpus callosum: genetic, developmental and functional aspects of connectivity. Nat Rev Neurosci 8:287–299.

Quigley M, Cordes D, Turski P, Moritz C, Haughton V, Seth R, Meyerand ME. 2003. Role of the corpus callosum in functional connectivity. AJNR Am J Neuroradiol 24:208–212.

Raichle ME, MacLeod AM, Snyder AZ, Powers WJ, Gusnard DA, Shulman GL. 2001. A default mode of brain function. Proc Natl Acad Sci U S A 98:676–682.

Saad ZS, Gotts SJ, Murphy K, Chen G, Jo HJ, Martin A, Cox RW. 2012. Trouble at rest: how correlation patterns and group differences become distorted after global signal regression. Brain Connectivity 2:25–32.

Skudlarski P, Jagannathan K, Calhoun VD, Hampson M, Skudlarska BA, Pearlson G. 2008. Measuring brain connectivity: diffusion tensor imaging validates resting state temporal correlations. Neuroimage 43:554–561.

Smith SM, Nichols TE. 2009. Threshold-free cluster enhancement: addressing problems of smoothing, threshold dependence and localisation in cluster inference. Neuroimage 44:83–98.

Smith SM, Fox PT, Miller KL, Glahn DC, Fox PM, Mackay CE, Filippini N, Watkins KE, Toro R, Laird AR, Beckmann CF. 2009. Correspondence of the brain's functional architecture during activation and rest. Proc Natl Acad Sci U S A 106:13040–13045.

Sporns O, Tononi G, Kotter R. 2005. The human connectome: a structural description of the human brain. PLoS Comput Biol 1:e42.

Stark D, Margulies D, Shehzad Z, Reiss P, Kelly AMC, Uddin L, Gee D, Roy A, Banich M, Castellanos FX, Milham M. 2008. Regional variation in interhemispheric coordination of intrinsic hemodynamic fluctuations. J Neurosci 28:13754–13764.

Tovar-Moll F, Moll J, de Oliveira-Souza R, Bramati I, Andreiuolo P, Lent R. 2007. Neuroplasticity in Human Callosal Dysgenesis: A Diffusion Tensor Imaging Study. Cereb Cortex 17:531–541.

Tyszka JM, Kennedy DP, Adolphs R, Paul LK. 2011. Intact bilateral resting-state networks in the absence of the corpus callosum. J Neurosci 31:15154–15162.

Uddin L, Mooshagian E, Zaidel E, Scheres A, Margulies D, Kelly AMC, Shehzad Z, Adelstein J, Castellanos FX, Biswal B, Milham M. 2008. Residual functional connectivity in the split-brain revealed with resting-state functional MRI. Neuro Report 19:703–709.

van den Heuvel M, Sporns O. 2011. Rich club organization of the human connectome. J Neurosci 31:15775–15786.

Van Dijk KR, Hedden T, Venkataraman A, Evans KC, Lazar SW, Buckner RL. 2010. Intrinsic functional connectivity as a tool for human connectomics: theory, properties, and optimization. J Neurophysiol 103:297–321.

Vanhaudenhuyse A, Boly M, Balteau E, Schnakers C, Moonen G, Luxen A, Lamy M, Degueldre C, Brichant JF, Maquet P, Laureys S, Faymonville ME. 2009. Pain and non-pain processing during hypnosis: a thulium-YAG event-related fMRI study. NeuroImage 47:1047–1054.

Wahl M, Strominger Z, Jeremy RJ, Barkovich AJ, Wakahiro M, *et al.* 2009. Variability of homotopic and heterotopic callosal connectivity in partial agenesis of the corpus callosum: a 3T diffusion tensor imaging and q-ball tractography study. AJNR Am J Neuroradiol 30:282–289.

Wang J-H, Zuo X-N, He Y. 2010. Graph-based network analysis of resting-state functional MRI. Front Syst Neurosci 4:16.

Wang J-H, Zuo X-N, Gohel S, Milham MP, Biswal BB, *et al.* 2011. Graph theoretical analysis of functional brain networks: test-retest evaluation on short- and long-term resting-state functional MRI data. PLoS One 6: e21976.

Yan CG, Cheung B, Kelly C, Colcombe S, Craddock RC, *et al.* 2013. A comprehensive assessment of regional variation in the impact of head micromovements on functional connectomics. Neuroimage 76:183–201.

Address correspondence to:
Pratik Mukherjee
Department of Radiology & Biomedical Imaging
University of California
185 Berry Street, Box 0946
San Francisco, CA 94107-0946

E-mail: pratik.mukherjee@ucsf.edu